Modulating the resistivity of MoS_2 through low energy phosphorus plasma implantation

K. Haynes, R. Murray, Z. Weinrich, X. Zhao, D. Chiappe, S. Sutar, I. Radu, C. Hatem, S. S. Perry, and K. S. Jones

Citation: Appl. Phys. Lett. **110**, 262102 (2017);
View online: https://doi.org/10.1063/1.4989829
View Table of Contents: http://aip.scitation.org/toc/apl/110/26
Published by the American Institute of Physics

Modulating the resistivity of MoS_2 through low energy phosphorus plasma implantation

K. Haynes,[1,a] R. Murray,[1] Z. Weinrich,[1] X. Zhao,[1] D. Chiappe,[2] S. Sutar,[2] I. Radu,[2] C. Hatem,[3] S. S. Perry,[1] and K. S. Jones[1]
[1]*Department of Materials Science and Engineering, University of Florida, Gainesville, Florida 32611, USA*
[2]*IMEC, Kapeldreef 75, 3001 Leuven, Belgium*
[3]*Applied Materials, Gloucester, Massachusetts 01930, USA*

(Received 31 March 2017; accepted 12 June 2017; published online 26 June 2017)

Molybdenum disulfide (MoS_2) is a promising potential replacement for Si in future microelectronic devices. Integration in electronic devices will likely involve the growth or transfer of large-area MoS_2 films onto substrates and subsequent isolation of devices. In this paper, the effect of ion implantation on the electrical properties of MoS_2 is reported. Large-area ~4 layer MoS_2 films were implanted by low energy phosphorus plasma at biases of 100, 200, and 300 V and a dose of 1×10^{14} cm^{-2}. Electrical measurements using patterned Ni/Au contacts show that after implantation, independent of bias, there is greater than a 10^4 increase in resistivity. TEM and Raman spectroscopy suggest that the film is crystalline prior to and after ion implantation and annealing and that there is no measurable sputtering following implantation. This suggests that the increase in resistivity is likely the result of radiation damage in the MoS_2. The thermal stability of the increase in electrical resistivity was assessed by a series of 15 min anneals beginning at 325 °C in a sulfur overpressure and progressing up to 525 °C under an Al_2O_3 ALD cap. The resistivity increase remained unchanged after annealing. These results suggest that implant isolation could provide a preferable alternative to reactive ion etching or chemical etching for electrical isolation of MoS_2. *Published by AIP Publishing.* [http://dx.doi.org/10.1063/1.4989829]

Molybdenum disulfide (MoS_2) is a two-dimensional (2D) transition metal dichalcogenide that has emerged as a promising electronic material over the past decade due to its tunable properties,[1,2] intrinsic bandgaps (1.29–1.9 eV),[3,4] lack of dangling bonds, high I_{ON}/I_{OFF} ratios (up to 10^9),[5] and carrier mobilities (20–200 cm^2/Vs).[6,7] These properties may enable the application of MoS_2 in electronic devices including field effect transistors,[7–9] p-n diodes,[10–12] and gas sensors.[13,14] Such integration will require the synthesis of high-quality, large-area MoS_2 films on a substrate and the fabrication of a high density of devices. Although development of such growth methods is ongoing,[15–17] relatively little attention has been given to the parallel development of device isolation schemes. Electrical isolation will be critical for these large-area films to prevent cross-talk between neighboring devices. This need has been overlooked so far because MoS_2 research has been largely based on the use of flakes produced by mechanical exfoliation or triangular islands produced by chemical vapor deposition. In these studies, single devices are fabricated on individual flakes, which are isolated by their nature. However, the practical implementation of MoS_2 devices on large-area films will require electrical isolation.

Although reactive ion etching or chemical etching could be used to create isolated channels,[18] these techniques can induce additional problems. Dangling bonds created at the edge sites are chemically active,[19] and edge sites can be metallic in nature,[20] negating the advantages of using a 2D material at short channel lengths. In addition, the exposed edges can allow liquids to intercalate between the MoS_2 and its substrate, overcoming the relatively weak van der Waals forces that bond them. This is most notably an issue with aqueous solutions due to the hydrophobic nature of aged synthetic MoS_2[21] and the hydrophilic nature of many of the substrates used with MoS_2 (SiO_2, sapphire, etc.). Aqueous solution processing, such as development during photolithography, can cause delamination of the free-standing MoS_2 channels from the substrate and subsequently cause mechanical damage to the films or even displacement of the entire channel. Indeed, some film transfer techniques rely on the ability of water to intercalate between MoS_2 and its substrate in order to separate them.[22,23] Although mineralogical flakes appear to be less sensitive to such energetic effects, the wetting properties of MoS_2 have been shown to be sensitive to a range of factors including number of layers, adsorption of hydrocarbons, and oxidation.[21] Short channel lengths are likely to increase the probability of delamination.

Ion implantation is a possible alternative to physical isolation. Ion implantation methods are commonly used for isolation in III-V devices.[24] The radiation damage caused by the implanted ions creates deep-level defects that trap charge carriers. These charge carriers cannot be thermally ionized from the defect states at room temperature, resulting in a significant increase in the sheet resistances of these materials. The increased resistance is stable up to the temperature at which these defects begin to anneal out of the crystal. This technique is widely used for its simplicity and ability to be used on a selected-area basis, in addition to its effectiveness. Initial studies of ion implantation on 2D materials suggest

[a]Author to whom correspondence should be addressed: kschuller@ufl.edu

that it is a compatible technique when used at sufficiently low energies.[25–28]

This work investigated low energy plasma implants of phosphorus into MoS_2. During plasma implantation, the implant energy can be controlled to low values (down to 0 eV) that result in shallow implant profiles that are appropriate for use with 2D materials. This implant system employs a radio frequency plasma source located in a chamber above the sample. The ions in the plasma are accelerated through an aperture toward the sample by a separate pulsed DC bias, resulting in a Gaussian beam that is swept over the sample. For this study, phosphine gas at a pressure of 5×10^{-6} Torr was used to generate the plasma, and a dose of 1×10^{14} cm^{-2} was used for all samples. To investigate the effect of different implant energies, three accelerating biases were chosen: 100 V, 200 V, and 300 V. Implant profiles generated using the Transport of Ions in Matter (TRIM) program, a free Monte Carlo simulation software (http://www.srim.org/), show that these biases result in a range of damage profiles [Fig. 1(b)]. For the 100 V implant, most of the energy is deposited near the surface of the film, while the energy deposition is more uniform through the film thickness for the 300 V implant. It should be noted that the actual profiles for the implants may have deviated somewhat from these simulations due to the distribution of beam angles through the aperture.

The large-area MoS_2 films [Fig. 1(a)] were synthesized through the sulfurization of the Mo metal on a sapphire substrate, a process that has been detailed elsewhere.[29] In short, a film of Mo is annealed at 800 °C for 30 min under flowing H_2S gas, resulting in the complete conversion of Mo into MoS_2. An additional annealing step after growth at 1000 °C for 20 min under H_2S/N_2 is performed to improve the crystallographic texture. The film is then transferred to a Si wafer with a 90-nm thermally grown layer of SiO_2.[22] The resulting MoS_2 film is ~4 trilayers thick and polycrystalline in nature with grain diameters ranging from 10 to 50 nm. A cross-sectional transmission electron microscope (TEM) image of the film before implant shows the individual trilayers preferentially aligned with the SiO_2 surface [Fig. 1(c)].

Samples were implanted for each of the three bias conditions. TEM following implant does not reveal measurable sputtering or visible structural disorder between the individual trilayers [Fig. 1(d)]. Photolithography was used to define the contact regions of transfer length method (TLM) structures [Fig. 2(a)]. Metal contacts of 30 nm Ni and 60 nm Au were formed by electron beam evaporation and liftoff. Large channel width-to-length ratios were used, allowing fringing resistances to be neglected for the non-patterned channels. Devices were capped with 30 nm of Al_2O_3 deposited at 200 °C by ALD [Fig. 2(b)]. Capping with a dielectric decreases Coulombic scattering, increasing the field effect mobility,[30] and also prevents the adsorption of gaseous molecules. Electrical measurements were performed using a Keithley 4200 Semiconductor Characterization System.

Output characteristics were measured for the three implanted samples and one non-implanted sample at each of the channel lengths d using drain voltage V_D sweeps from −1 to 1 V. No bias was applied to the bottom gate for these measurements. Representative curves for a single channel length are shown in Fig. 2(c). The I–V characteristics show relatively symmetrical current response in this voltage range for both implanted and non-implanted samples, despite the known existence of a Schottky barrier at Ni–MoS_2 interfaces.[5,31] The resistances of the implanted samples are markedly higher than that of the non-implanted sample, as shown in the inset of Fig. 2(c). For the 32 μm channel length shown, the resistance of the non-implanted sample is 1.9×10^6 $\Omega \cdot \mu$m in comparison to 1.6×10^{10}–3.6×10^{11} $\Omega \cdot \mu$m for the implanted samples. There does not appear to be a systematic difference in resistance among the 100, 200, and 300 V implants.

TLM structures were also measured in order to deconvolve sheet resistance and contact resistance. Because it is proportional to the y-intercept of the linear regression, contact resistance was found to be sensitive to small variations between data points for the longer channel lengths. This prevented accurate determination of the contact resistance. Sheet resistance, which is proportional to the slope of the linear regression, was consistent however. As shown in Fig. 2(d), the sheet resistance of the non-implanted sample is several orders of magnitude lower than that of the implanted samples: 6.1×10^4 Ω/□ compared to 1.6×10^9 Ω/□ for the 200 V implant. Sheet resistances of the 100 V and 300 V samples are similar to that of the 200 V sample. Using the average film thickness determined from cross-sectional TEM (2.7 nm), it is found that these values correspond to resistivities of 1.6×10^{-2} Ω·cm and 4.3×10^2 Ω·cm. The resistivities of all the samples are summarized in Fig. 2(e). Error bars were calculated for each sample by performing two separate linear regressions using the lowest resistance values and the highest resistance values for each channel length.

Raman analysis of the non-implanted and implanted samples shows that the primary E^1_{2g} and A_{1g} modes are maintained after implant (Fig. 3). These modes correspond to the

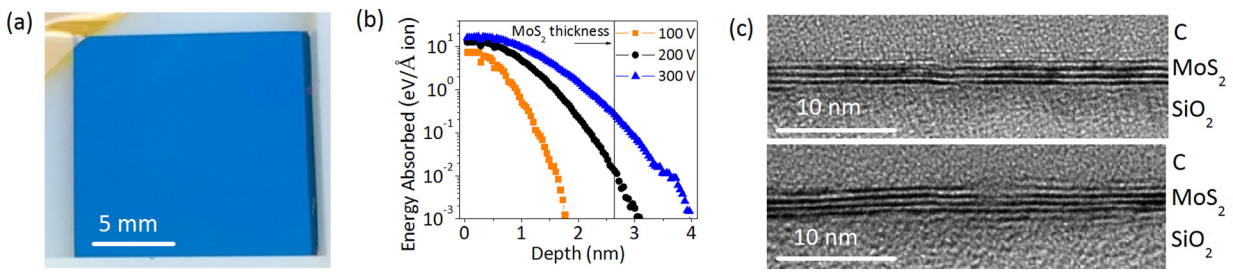

FIG. 1. (a) Photograph of the large-area, synthesized MoS_2 film. (b) TRIM simulation of the energy deposited during implant as a function of depth for the three implant biases: 100 V, 200 V, and 300 V. The average thickness of the film (~4 trilayers) is indicated by the black line. (c) Cross-sectional TEM images of the MoS_2 film before implant and (d) after a 200 V plasma implant. The carbon is a protective layer for sample preparation.

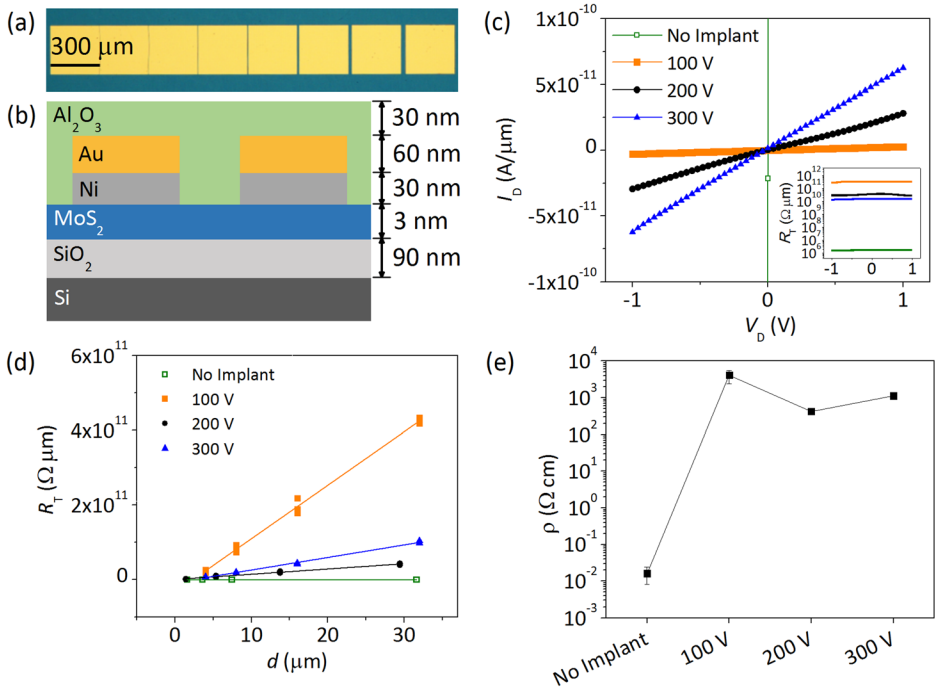

FIG. 2. (a) An optical image of a series of TLM devices on the MoS_2 film. (b) A cross-sectional illustration of the device stack. (c) Output characteristics for a 32 μm channel length for the four samples show the suppression of current after implant. (Inset) Resistance vs. drain voltage for the same samples. (d) A plot of the TLM data reveals the orders of magnitude between the resistances of the non-implanted and implanted samples. Lines are linear regressions. (e) A summary of the resistivities extracted from the TLM data. Error bars indicate the range of resistivities that were extracted by fitting a select range of data points. Error bars that are not visible are smaller than the height of the data symbol.

in-plane vibration of Mo and S atoms and the out-of-plane vibration of S atoms. Increased structural disorder is indicated by the appearance of a shoulder on the E^1_{2g} peak and increased full width at half maximums (FWHMs) for the implanted samples relative to the non-implanted sample. For example, FWHMs for the E^1_{2g} peak are 4.88, 8.05, 8.19, and 9.82 cm^{-1} for the non-implanted, 100 V, 200 V, and 300 V samples, respectively. Correspondingly, the FWHMs for the A_{1g} peak are 4.49, 6.44, 6.39, and 6.80, respectively. In addition, the appearance of a peak at 225 cm^{-1} suggests the occurrence of some oxidation of the film and the formation of Mo–O bonds.[32,33] The formation of MoO_3 in MoS_2 has been shown to occur in sputtered MoS_2 after exposure to atmospheric conditions[34] and increased resistivity may be associated with strain in the MoS_2 due to lattice mismatch with MoO_3.[32] This could partially account for the increased resistance of the implanted films. Finally, softening of both peaks is observed: $\sim$1.0 cm^{-1} for E^1_{2g} and $\sim$0.5 cm^{-1} for A_{1g}. The A_{1g} mode is sensitive to doping due to strong electron-phonon coupling, and softening can be associated with electron doping.[35] Conversely, stiffening of this mode has been tied to p-type doping of MoS_2.[36,37] This is an important point because P could act as a p-type dopant on S sites in MoS_2,[26,38] compensating the naturally n-type MoS_2. However, the softening of the A_{1g} mode observed here is inconsistent with p-type doping, excluding the possibility of dopant compensation as an explanation for the increased resistivity.

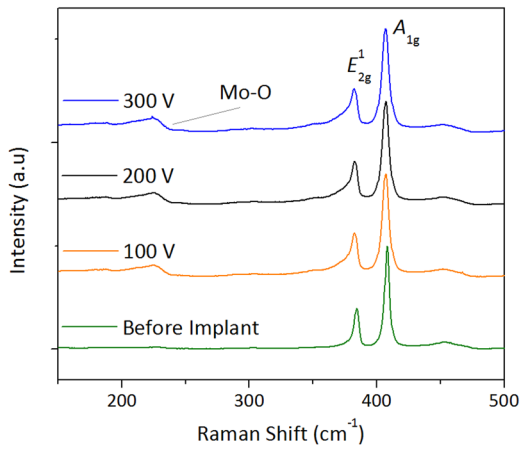

FIG. 3. Raman spectra for the four samples. FWHMs have increased for the two primary modes and an additional peak corresponding to Mo–O bonds at 225 cm^{-1} has formed for the implanted samples.

The thermal stability of the increased resistivity is an important property of any isolation mechanism. Here, the stability was assessed by a series of anneals beginning at 325 °C under a sulfur overpressure and progressing up to 525 °C under an ALD cap. For simplicity, only the 200 V implant was investigated, as it represents the midpoint of the biases studied, and no significant differences were observed in the electrical properties of the three different biases. The first anneal was performed after implant but before device fabrication. The sample was sealed in a Pyrex ampoule with a small amount of sulfur powder under a low vacuum (5×10^{-3} torr). The ampoule was then annealed at 325 °C for 15 min. The pressure created by the sulfur powder at the annealing temperature was estimated to be 100 Torr. Similar anneals at 325 °C in the presence of a sulfur-containing solution have been shown to reduce the number of sulfur vacancies.[39] Raman analysis on the implanted and annealed sample shows improved FWHMs of 7.08 cm^{-1} for E^1_{2g} and 5.82 cm^{-1} for A_{1g}. However, the TLM results reveal a slight increase in resistivity from 3.1×10^2 to 8.0×10^2 Ω·cm (Fig. 4). This increase is minor when compared to the increase that was observed after implant. Additional anneals were performed on the same devices under an ALD cap. After 15 min at 425 °C and then 15 min at 525 °C, the sheet resistance remained largely unchanged, with only a slight decrease approaching the as-implanted sheet resistance value. These results indicate that the increase in resistance is

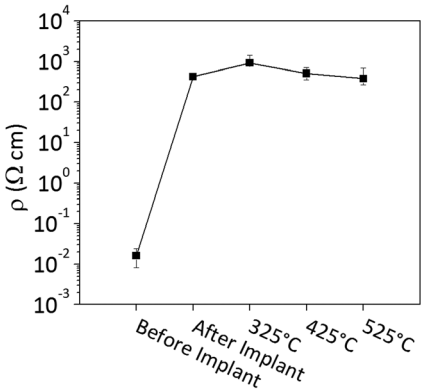

FIG. 4. A summary of the resistivities extracted from TLM of the annealed samples.

stable up to 525 °C. Higher temperatures were not explored in this case because of the reactivity and diffusion of the other materials in the device at higher temperatures.

In conclusion, low energy phosphorus plasma implantation was found to increase the resistivity of a synthetic MoS_2 film by more than four orders of magnitude. This increase in resistivity was stable up to at least 525 °C. Similar resistivities for all three bias conditions (100 V, 200 V, and 300 V) and softening of the A_{1g} mode suggest that higher resistivity is associated with radiation damage from the implant rather than dopant compensation. Raman and TEM show that crystallography is largely maintained without measurable sputtering, a departure from previous plasma-based processing of MoS_2.[26,40,41] This is likely due to differences in dose (which was not directly measured in previous reports), plasma species, location of the plasma generation relative to the sample (remote vs. immersion), and implant energies. Raman also reveals partial oxidation of the MoS_2, suggesting that strain from lattice mismatch with MoO_x could play a role in the increased resistivity, as shown in other implant and radiation damage studies.[32,33] These results suggest that plasma implantation can be used to alter the resistivity of MoS_2 and may offer an alternative method for device isolation.

This work was funded through a research grant by Applied Materials. The authors acknowledge the Research Service Center at the University of Florida for the use of their clean room facilities. The authors further wish to thank IMEC for providing the films for implant and Applied Materials for performing the implants.

[1]J. Ryou, Y.-S. Kim, S. KC, and K. Cho, Sci. Rep. **6**, 29184 (2016).
[2]T. Chu, H. Ilatikhameneh, G. Klimeck, R. Rahman, and Z. Chen, Nano Lett. **15**, 8000 (2015).
[3]G. L. Frey, S. Elani, M. Homyonfer, Y. Feldman, and R. Tenne, Phys. Rev. B **57**, 6666 (1998).
[4]K. F. Mak, C. Lee, J. Hone, J. Shan, and T. F. Heinz, Phys. Rev. Lett. **105**, 136805 (2010).
[5]H. Liu, A. T. Neal, and P. D. Ye, ACS Nano **6**, 8563 (2012).
[6]D. Lembke, A. Allain, and A. Kis, Nanoscale **7**, 6255 (2015).
[7]B. Radisavljevic, A. Radenovic, J. Brivio, V. Giacometti, and A. Kis, Nat. Nanotechnol. **6**, 147 (2011).
[8]H. Chang, S. Yang, J. Lee, L. Tao, W. Hwang, D. Jena, N. Lu, and D. Akinwande, ACS Nano **7**, 5446 (2013).
[9]S. Kim, A. Konar, W.-S. Hwang, J. H. Lee, J. Lee, J. Yang, C. Jung, H. Kim, J.-B. Yoo, J.-Y. Choi, Y. W. Jin, S. Y. Lee, D. Jena, W. Choi, and K. Kim, Nat. Commun. **3**, 1011 (2012).
[10]Q.-Q. Sun, Y.-J. Li, J.-L. He, W. Yang, P. Zhou, H.-L. Lu, S.-J. Ding, and D. W. Zhang, Appl. Phys. Lett. **102**, 93104 (2013).
[11]M. S. Choi, D. Qu, D. Lee, X. Liu, K. Watanabe, T. Taniguchi, and W. J. Yoo, ACS Nano **8**, 9332 (2014).
[12]J. Suh, T. E. Park, D. Y. Lin, D. Fu, J. Park, H. J. Jung, Y. Chen, C. Ko, C. Jang, Y. Sun, R. Sinclair, J. Chang, S. Tongay, and J. Wu, Nano Lett. **14**, 6976 (2014).
[13]H. Ul Hassan, J. Mun, B. S. Kang, J. Y. Song, T. Kim, and S.-W. Kang, RSC Adv. **6**, 75839 (2016).
[14]H. Li, Z. Yin, Q. He, H. Li, X. Huang, G. Lu, D. W. H. Fam, A. I. Y. Tok, Q. Zhang, and H. Zhang, Small **8**, 63 (2012).
[15]Y.-H. Lee, X.-Q. Zhang, W. Zhang, M.-T. Chang, C.-T. Lin, K.-D. Chang, Y.-C. Yu, J. T.-W. Wang, C.-S. Chang, L.-J. Li, and T.-W. Lin, Adv. Mater. **24**, 2320 (2012).
[16]Y. Lee, J. Lee, H. Bark, I.-K. Oh, G. H. Ryu, Z. Lee, H. Kim, J. H. Cho, J.-H. Ahn, and C. Lee, Nanoscale **6**, 2821 (2014).
[17]Y. Feng, K. Zhang, F. Wang, Z. Liu, M. Fang, R. Cao, Y. Miao, Z. Yang, W. Mi, Y. Han, Z. Song, and H. S. P. Wong, ACS Appl. Mater. Interfaces **7**, 22587 (2015).
[18]N. Ninomiya, T. Mori, N. Uchida, E. Watanabe, D. Tsuya, S. Moriyama, M. Tanaka, and A. Ando, Jpn. J. Appl. Phys. **54**, 46502 (2015).
[19]T. F. Jaramillo, K. P. Jørgensen, J. Bonde, J. H. Nielsen, S. Horch, and I. Chorkendorff, Science **317**, 100 (2007).
[20]M. V. Bollinger, J. V. Lauritsen, K. W. Jacobsen, J. K. Nørskov, S. Helveg, and F. Besenbacher, Phys. Rev. Lett. **87**, 196803 (2001).
[21]P. K. Chow, E. Singh, B. C. Viana, J. Gao, J. Luo, J. Li, Z. Lin, A. L. Elías, Y. Shi, Z. Wang, M. Terrones, and N. Koratkar, ACS Nano **9**, 3023 (2015).
[22]A. Gurarslan, Y. Yu, L. Su, Y. Yu, F. Suarez, S. Yao, Y. Zhu, M. Ozturk, Y. Zhang, and L. Cao, ACS Nano **8**, 11522 (2014).
[23]D. Ma, J. Shi, Q. Ji, K. Chen, J. Yin, Y. Lin, Y. Zhang, M. Liu, Q. Feng, X. Song, X. Guo, J. Zhang, Y. Zhang, and Z. Liu, Nano Res. **8**, 3662 (2015).
[24]S. J. Pearton, Mater. Sci. Rep. **4**, 313 (1990).
[25]R. Murray, K. Haynes, X. Zhao, S. Perry, C. Hatem, and K. Jones, ECS J. Solid State Sci. Technol. **5**, Q3050 (2016).
[26]A. Nipane, D. Karmakar, N. Kaushik, S. Karande, and S. Lodha, ACS Nano **10**, 2128 (2016).
[27]U. Bangert, W. Pierce, D. M. Kepaptsoglou, Q. Ramasse, R. Zan, M. H. Gass, J. A. Van den Berg, C. B. Boothroyd, J. Amani, and H. Hofsäss, Nano Lett. **13**, 4902 (2013).
[28]A. Azcatl, X. Qin, A. Prakash, C. Zhang, L. Cheng, Q. Wang, N. Lu, M. J. Kim, J. Kim, K. Cho, R. Addou, C. L. Hinkle, J. Appenzeller, and R. M. Wallace, Nano Lett. **16**, 5437 (2016).
[29]D. Chiappe, I. Asselberghs, S. Sutar, S. Iacovo, V. Afanas'ev, A. Stesmans, Y. Balaji, L. Peters, M. Heyne, M. Mannarino, W. Vandervorst, S. Sayan, C. Huyghebaert, M. Caymax, M. Heyns, S. De Gendt, I. Radu, and A. Thean, Adv. Mater. Interfaces **3**, 1500635 (2016).
[30]D. Jena and A. Konar, Phys. Rev. Lett. **98**, 136805 (2007).
[31]S. Das, H.-Y. Chen, A. V. Penumatcha, and J. Appenzeller, Nano Lett. **13**, 100 (2013).
[32]M. R. Islam, N. Kang, U. Bhanu, H. P. Paudel, M. Erementchouk, L. Tetard, M. N. Leuenberger, and S. I. Khondaker, Nanoscale **6**, 10033 (2014).
[33]N. Choudhary, M. R. Islam, N. Kang, L. Tetard, Y. Jung, and S. I. Khondaker, J. Phys.: Condens. Matter **28**, 364002 (2016).
[34]T. B. Stewart and P. D. Fleischauer, Inorg. Chem. **21**, 2426 (1982).
[35]B. Chakraborty, A. Bera, D. V. S. Muthu, S. Bhowmick, U. V. Waghmare, and A. K. Sood, Phys. Rev. B **85**, 161403 (2012).
[36]A. Tarasov, S. Zhang, M.-Y. Tsai, P. M. Campbell, S. Graham, S. Barlow, S. R. Marder, and E. M. Vogel, Adv. Mater. **27**, 1175 (2015).
[37]P. Mishra, M. Tangi, T. K. Ng, M. N. Hedhili, D. H. Anjum, M. S. Alias, C.-C. Tseng, L.-J. Li, and B. S. Ooi, Appl. Phys. Lett. **110**, 12101 (2017).
[38]K. Dolui, I. Rungger, C. D. Pemmaraju, and S. Sanvito, Phys. Rev. B **88**, 75420 (2013).
[39]Q. Ma, M. Isarraraz, C. S. Wang, E. Preciado, V. Klee, S. Bobek, K. Yamaguchi, E. Li, P. M. Odenthal, A. Nguyen, D. Barroso, D. Sun, G. von Son Palacio, M. Gomez, A. Nguyen, D. Le, G. Pawin, J. Mann, T. F. Heinz, T. S. Rahman, and L. Bartels, ACS Nano **8**, 4672 (2014).
[40]M. Chen, H. Nam, S. Wi, L. Ji, X. Ren, L. Bian, S. Lu, and X. Liang, Appl. Phys. Lett. **103**, 142110 (2013).
[41]S. Wi, H. Kim, M. Chen, H. Nam, L. J. Guo, E. Meyhofer, and X. Liang, ACS Nano **8**, 5270 (2014).